THE ASTROPHYSICAL JOURNAL, 471:737–747, 1996 November 10

OPTICAL CONTINUUM AND EMISSION-LINE VARIABILITY OF THE SEYFERT 1 GALAXY MARKARIAN 509

T. E. CARONE,[1,2] B. M. PETERSON,[3] J. BECHTOLD,[1] R. BERTRAM,[3,4] K. BISCHOFF,[5] M. DIETRICH,[6]
A. V. FILIPPENKO,[7] L. C. HO,[7,8] J. P. HUCHRA,[8] W. KOLLATSCHNY,[5] K. T. KORISTA,[3,9,10]
T. MATHESON,[7] R. W. POGGE,[3] J. C. SHIELDS,[1,7,11,12] P. S. SMITH,[1]
R. M. WAGNER,[3,4] AND B. J. WILKES[8]

Received 1996 March 17; accepted 1996 June 10

ABSTRACT

We report on the results of a 5 year coordinated program of spectroscopic monitoring of the luminous Seyfert 1 galaxy Markarian 509. The Hβ and He II λ4686 emission lines are found to respond to continuum variations with time lags of $\sim$80 and $\sim$60 days, respectively, considerably longer than the emission-line lags measured for other Seyfert galaxies.

Subject headings: galaxies: active — galaxies: individual (Markarian 509) — galaxies: Seyfert

1. INTRODUCTION

Over the last several years, great progress in probing the central environment of active galactic nuclei (AGNs) has been made by use of "reverberation mapping" techniques (Blandford & McKee 1982), whereby the geometry and kinematics of the broad-line region (BLR) can be inferred from the detailed response of the broad emission lines to continuum variations (see Peterson 1993, 1994 for recent reviews).

Most of the AGNs that have been monitored closely thus far are nearby Seyfert 1 galaxies that have a known history of continuum and emission-line variability, although higher luminosity AGNs (quasars) are now beginning to receive more attention (e.g., Maoz et al. 1994; Maoz 1994; Erkens et al. 1995). Determination of the emission-line response times (or "lags") for higher luminosity sources is of particular interest because it affords a test of photoionization models of the BLR. For simple photoionization models, the approximate similarity of AGN broad-line spectra implies that the ionization parameter U (i.e., the ratio of ionizing photons to particles at the inward face of a line-emitting cloud) and particle density in the BLR do not vary strongly with luminosity. If the *shape* of AGN ionizing continua is also independent of luminosity, one is led directly to the simple and testable prediction that the size of the BLR r should scale with luminosity L as

$$r \propto L^{1/2} . \quad (1)$$

In this paper, we describe the initial results of a 5 year intensive monitoring program on the luminous Seyfert 1 galaxy Markarian (Mrk) 509. While the apparent magnitude ($B \approx 13.9$ mag) of Mrk 509 is similar to those of other AGNs that have been monitored intensively, it is more distant than the other well monitored sources ($z \approx 0.034$) and intrinsically more luminous, with an absolute magnitude $M_B \approx -21.1 + 5 \log h$, where h is the Hubble constant in units of 100 km s^{-1} Mpc^{-1}; this is nearly an order of magnitude more luminous than most of the other well studied sources, and only 0.4 mag fainter than the (arbitrary) division in luminosity between Seyfert galaxies and quasars, as defined by Schmidt & Green (1983), i.e., $M_B(\mathrm{QSOs}) \leq -21.5 + 5 \log h$.

The observations described in § 2 were made whenever Mrk 509 was accessible between 1988 September and 1993 December with a number of different telescopes. Many of these observations were obtained while the observers were also engaged in a coordinated monitoring of the Seyfert 1 galaxy NGC 5548 (Peterson et al. 1991, 1992, 1994; Korista et al. 1995). Because several different instruments were used in these observations, the separate data sets, although internally homogeneous, need to be adjusted to a common scale to correct for differences that we attribute primarily to aperture effects (e.g., see Peterson et al. 1995). The intercalibration process and methods of measurement are described in § 3. The principal results of this variability study are presented in § 4 and discussed briefly in § 5.

2. OBSERVATIONS

A complete log of optical spectroscopic observations appears in Table 1. Columns (1) and (2) give the UT date and Julian date, respectively, of each observation. Column (3) indicates the telescope and instrument that was used to obtain each spectrum. The projected spectrograph entrance aperture, in arcseconds, is given in column (4). The first dimension is the slit width in the dispersion direction, and the second dimension is the slit length in the cross-dispersion direction; for CCDs, the latter dimension is the "extraction window" used in the reduction to one dimension. The slit position angle is given in column (5), measured eastward from north; the cross-dispersion direction runs north to south for a position angle 0°. An estimate of the seeing, when it was recorded at the telescope, is given in column (6). In the case of the Ohio State spectra (set "A"),

[1] Steward Observatory, University of Arizona, Tucson, AZ 85721.
[2] Current address: 28740 West Fox River Drive, Cary, IL 60013.
[3] Department of Astronomy, The Ohio State University, 174 West 18th Avenue, Columbus, OH 43210.
[4] Mailing address: Lowell Observatory, Mars Hill Road, 1400 West, Flagstaff, AZ 86001.
[5] Universitäts-Sternwarte Göttingen, Geismarlandstrasse 11, D-37083 Göttingen, Germany.
[6] Landessternwarte, Königstuhl, D-69117 Heidelberg, Germany.
[7] Department of Astronomy, University of California, Berkeley, CA 94720.
[8] Harvard-Smithsonian Center for Astrophysics, 60 Garden Street, Cambridge, MA 02138.
[9] Observatories of the Carnegie Institution of Washington, 813 Santa Barbara Street, Pasadena, CA 91101.
[10] Department of Physics and Astronomy, University of Kentucky, Lexington, KY 40506.
[11] Hubble Fellow.
[12] Present address: Department of Physics and Astronomy, Ohio University, Clippinger Research Labs. 251B, Athens, OH 45701.

TABLE 1

LOG OF SPECTROSCOPIC OBSERVATIONS

UT DATE (1)	JULIAN DATE (2)	CODE (3)	APERTURE Size (arcsecond) (4)	APERTURE P.A. (degree) (5)	SEEING (arcsecond) (6)	RESOLUTION (Å) (7)	RANGE (Å) (8)	IRAF FILE (9)
1988 Sep 11	2447415	B	3.2 × 6.4	90	...	5	4550–7000	m57415b
1988 Sep 16	2447420	B	3.2 × 6.4	90	...	5	4550–7000	m57420b
1988 Sep 17	2447421	B	3.2 × 6.4	90	...	5	4550–7000	m57421b
1988 Oct 8	2447442	B	3.2 × 6.4	90	...	5	4550–7000	m57442b
1988 Oct 12	2447446	B	3.2 × 6.4	90	...	5	4550–7000	m57446b
1988 Nov 7	2447472	B	3.2 × 6.4	90	...	5	4550–7000	m57472b
1988 Nov 13	2447478	B	3.2 × 6.4	90	...	5	4550–7000	m57478b
1988 Dec 2	2447497	B	3.2 × 6.4	90	...	5	4590–7000	m57497b
1988 Dec 3	2447498	B	3.2 × 6.4	90	...	5	4550–7000	m57498b
1988 Dec 5	2447500	B	3.2 × 6.4	90	...	5	4590–7000	m57500b
1988 Dec 6	2447501	B	3.2 × 6.4	90	...	5	4590–7000	m57501b
1989 May 7	2447653	A	5.0 × 7.6	90	>5	9	4450–5400	m57653a
1989 May 11	2447657	A	5.0 × 7.6	90	>5	9	4470–5600	m57657a
1989 May 17	2447663	F	2.1 × 7.0	90	2.0	5	4000–5530	m57663fa
1989 May 17	2447663	F	2.1 × 7.0	90	2.0	5	5640–7150	m57663fb
1989 May 18	2447664	F	2.1 × 7.0	90	1.5–2	5	4750–5300	m57664fa
1989 May 18	2447664	F	2.1 × 7.0	90	1.5–2	5	6500–6990	m57664fb
1989 Jun 1	2447678	A	5.0 × 7.6	90	>5	9	4450–5400	m57678a
1989 Jun 27	2447704	E	4.5 × 27.2	90	...	14	3200–5800	m57704ea
1989 Jun 27	2447704	E	4.5 × 27.2	90	...	4	4430–5150	m57704eb
1989 Jun 27	2447704	E	4.5 × 27.2	90	...	14	5680–8270	m57704ec
1989 Jul 10	2447717	B	3.2 × 6.4	90	...	5	4550–7000	m57717b
1989 Aug 29	2447767	E	4.5 × 27.2	90	...	14	3300–5900	m57767ea
1989 Aug 29	2447767	E	4.5 × 27.2	90	...	4	4440–5180	m57767eb
1989 Aug 29	2447767	E	4.5 × 27.2	90	...	14	5720–8600	m57704ec
1989 Sep 8	2447777	B	3.2 × 6.4	90	...	5	4550–7000	m57777b
1989 Sep 9	2447778	E	4.5 × 27.2	90	...	14	3740–5900	m57778ea
1989 Sep 9	2447778	E	4.5 × 27.2	90	...	14	5750–8630	m57778eb
1989 Sep 10	2447779	E	4.5 × 27.2	90	...	14	3450–5900	m57779ea
1989 Sep 10	2447779	E	4.5 × 27.2	90	...	4	4440–5230	m57779eb
1989 Sep 10	2447779	E	4.5 × 27.2	90	...	14	5740–8630	m57779ec
1989 Sep 14	2447783	A	5.0 × 7.6	90	4.0	9	4570–5670	m57783a
1989 Sep 19	2447788	A	5.0 × 7.6	90	4.6	9	4580–5720	m57788a
1989 Sep 29	2447798	B	3.2 × 6.4	90	...	5	4550–7000	m57798b
1989 Sep 30	2447799	B	3.2 × 6.4	90	...	5	4550–7000	m57799b
1989 Oct 1	2447800	B	3.2 × 6.4	90	...	5	4550–7000	m57800b
1989 Oct 6	2447805	B	3.2 × 6.4	90	...	5	4550–7000	m57805b
1989 Oct 17	2447816	A	5.0 × 7.6	90	4.6	9	4510 –5640	m57816a
1989 Oct 24	2447823	B	3.2 × 6.4	90	...	5	4550–7000	m57823b
1989 Oct 25	2447824	B	3.2 × 6.4	90	...	5	4550–7000	m57824b
1989 Oct 26	2447826	F	2.0 × 7.0	90	2.0	5	4130–7440	m57826f
1989 Oct 27	2447826	B	3.2 × 6.4	90	...	5	4550–7000	m57826b
1989 Oct 30	2447829	B	3.2 × 6.4	90	...	5	4550–7000	m57829b
1989 Nov 1	2447831	A	5.0 × 7.6	90	5.0	9	4550–5630	m57831a
1989 Nov 1	2447831	B	3.2 × 6.4	90	...	5	4550–7000	m57831b
1989 Nov 2	2447832	B	3.2 × 6.4	90	...	5	4550–7000	m57832b
1989 Nov 3	2447833	B	3.2 × 6.4	90	...	5	4550–7000	m57833b
1989 Nov 4	2447834	B	3.2 × 6.4	90	...	5	4550–7000	m57834b
1989 Nov 5	2447835	B	3.2 × 6.4	90	...	5	4550–7000	m57835b
1989 Nov 7	2447837	A	5.0 × 7.6	90	4.2	9	4590–5700	m57837a
1989 Nov 16	2447846	A	5.0 × 7.6	90	4.1	9	4570–5710	m57846a
1989 Nov 22	2447852	A	5.0 × 7.6	90	5.3	9	4570–5720	m57852a
1989 Nov 29	2447859	B	3.2 × 6.4	90	...	5	4550–7000	m57859b
1989 Dec 8	2447868	A	5.0 × 7.6	90	4.5	9	4590–5730	m57868a
1990 May 9	2448020	A	5.0 × 7.6	90	4.4	9	4520–5690	m58020a
1990 May 26	2448037	A	5.0 × 7.6	90	3.5	9	4540–5670	m58037a
1990 Jun 2	2448044	A	5.0 × 7.6	90	5.5	9	4290–5430	m58044a
1990 Jun 17	2448059	B	3.2 × 6.4	90	...	5	4570–7000	m58059b
1990 Jun 18	2448060	B	3.2 × 6.4	90	...	5	4600–7000	m58060b
1990 Jun 19	2448061	A	5.0 × 7.6	90	3.6	9	4520–5660	m58061a
1990 Jun 19	2448061	B	3.2 × 6.4	90	...	5	4580–7000	m58061b
1990 Jun 22	2448064	B	3.2 × 6.4	90	...	5	4580–7000	m58064b
1990 Jun 23	2448065	B	3.2 × 6.4	90	...	5	4590–7000	m58065b
1990 Jun 26	2448068	A	5.0 × 7.6	90	4.0	9	4510–5650	m58068a
1990 Jul 5	2448077	A	5.0 × 7.6	90	3.4	9	4430–5570	m58077a
1990 Jul 16	2448088	F	2.0 × 7.0	90	2–3	5	4000–7280	m58088f
1990 Jul 18	2448090	A	5.0 × 7.6	90	3.6	9	4470–5610	m58090a
1990 Jul 30	2448102	D	8.0 × 8.0	20	1–1.5	10	3250–9700	m58102d
1990 Aug 9	2448112	A	5.0 × 7.6	90	3.4	9	4530–5670	m58112a

TABLE 1—*Continued*

UT Date (1)	Julian Date (2)	Code (3)	Aperture Size (arcsecond) (4)	Aperture P.A. (degree) (5)	Seeing (arcsecond) (6)	Resolution (Å) (7)	Range (Å) (8)	IRAF File (9)
1990 Aug 25	2448128	A	5.0 × 7.6	90	4.1	9	4520–5650	m58128a
1990 Sep 9	2448143	A	5.0 × 7.6	90	2.3	9	4530–5670	m58143a
1990 Sep 14	2448148	A	5.0 × 7.6	90	3.0	9	4540–5680	m58148a
1990 Sep 15	2448149	A	5.0 × 7.6	90	3.8	9	4600–5690	m58149a
1990 Sep 17	2448151	A	5.0 × 7.6	90	2.7	9	4530–5670	m58151a
1990 Sep 17	2448151	B	3.2 × 6.4	90	…	5	4580–7000	m58151b
1990 Sep 26	2448160	A	5.0 × 7.6	90	1.8	9	4540–5680	m58160a
1990 Sep 27	2448161	D	10.0 × 10.0	20	2	20	3940–9680	m58161d
1990 Sep 28	2448162	B	3.2 × 6.4	90	…	5	4580–7000	m58162b
1990 Oct 11	2448175	A	5.0 × 7.6	90	>5	9	4520–5660	m58175a
1990 Oct 15	2448179	A	5.0 × 7.6	90	2.4	9	4540–5680	m58179a
1990 Oct 15	2448179	B	3.2 × 6.4	90	…	5	4600–7000	m58179b
1990 Oct 20	2448184	D	10.0 × 10.0	10	2–3	20	3140–9690	m58184d
1990 Oct 23	2448187	A	5.0 × 7.6	90	3.0	9	4510–5640	m58187a
1990 Oct 23	2448187	B	3.2 × 6.4	90	…	5	4600–7000	m58187b
1990 Oct 24	2448188	B	3.2 × 6.4	90	…	5	4600–7000	m58188b
1990 Oct 25	2448189	B	3.2 × 6.4	90	…	5	4600–7000	m58189b
1990 Oct 29	2448193	A	5.0 × 7.6	90	4.8	9	4520–5650	m58193a
1990 Nov 5	2448200	A	5.0 × 7.6	90	4.8	9	4530–5670	m58200a
1990 Nov 11	2448206	D	10.0 × 10.0	37	1.5–2	20	3350–9780	m58206d
1990 Nov 12	2448207	A	5.0 × 7.6	90	3.4	9	4530–5670	m58207a
1990 Nov 25	2448220	A	5.0 × 7.6	90	4.0	9	4540–5670	m58220a
1990 Nov 28	2448223	C	8.0 × 9.0	43	3	9	3480–9980	m58223c
1990 Dec 5	2448230	A	5.0 × 7.6	90	4.4	9	4550–5670	m58230a
1990 Dec 11	2448236	A	5.0 × 7.6	90	3.0	9	4530–5670	m58236a
1991 Jun 14	2448421	A	5.0 × 7.6	90	4.2	9	4470–5600	m58421a
1991 Jun 24	2448431	A	5.0 × 7.6	90	4.7	9	4530–5660	m58431a
1991 Jul 19	2448456	A	5.0 × 7.6	90	3.2	9	4520–5650	m58456a
1991 Jul 23	2448460	A	5.0 × 7.6	90	2.8	9	4520–5650	m58460a
1991 Aug 4	2448472	D	4.0 × 10.0	20	1.5	20	3200–9800	m58472d
1991 Aug 19	2448487	D	4.0 × 10.0	13	1	20	3250–9800	m58487d
1991 Sep 13	2448512	A	5.0 × 7.6	90	2.8	9	4560–5650	m58512a
1991 Sep 14	2448513	A	5.0 × 7.6	90	4.0	9	4550–5640	m58513a
1991 Sep 15	2448514	A	5.0 × 7.6	90	4.1	9	4560–5650	m58514a
1991 Sep 17	2448516	A	5.0 × 7.6	90	4.1	9	4560–5650	m58516a
1991 Sep 21	2448520	A	5.0 × 7.6	90	3.1	9	4540–5630	m58512a
1991 Oct 5	2448534	A	5.0 × 7.6	90	2.8	9	4540–5630	m58534a
1992 Apr 21	2448733	A	5.0 × 7.6	90	3.9	9	4530–5680	m58733a
1992 Jun 7	2448780	A	5.0 × 7.6	90	3.9	9	4540–5700	m58780a
1992 Jun 16	2448789	A	5.0 × 7.6	90	3.7	9	4550–5710	m58789a
1992 Jun 23	2448796	A	5.0 × 7.6	90	3.3	9	4490–5650	m58796a
1992 Jun 25	2448798	D	4.0 × 10.0	61	2.5	10	3300–8200	m58798d
1992 Jul 7	2448810	A	5.0 × 7.6	90	1.4	9	4540–5700	m58810a
1992 Jul 14	2448817	A	5.0 × 7.6	90	3.2	9	4550–5720	m58817a
1992 Jul 22	2448825	A	5.0 × 7.6	90	2.8	9	4540–5700	m58825a
1992 Aug 5	2448839	A	5.0 × 7.6	90	>5	9	4570–5730	m58839a
1992 Aug 14	2448848	A	5.0 × 7.6	90	2.2	9	4510–5670	m58848a
1992 Aug 28	2448862	A	5.0 × 7.6	90	2.6	9	4560–5710	m58862a
1992 Sep 4	2448869	A	5.0 × 7.6	90	2.7	9	4530–5680	m58869a
1992 Sep 11	2448876	A	5.0 × 7.6	90	2.4	9	4570–5720	m58876a
1992 Sep 18	2448883	A	5.0 × 7.6	90	2.4	9	4540–5700	m58883a
1992 Sep 24	2448889	A	5.0 × 7.6	90	2.7	9	4500–5660	m58889a
1992 Oct 3	2448898	A	5.0 × 7.6	90	2.9	9	4510–5670	m58898a
1992 Oct 10	2448904	A	5.0 × 7.6	90	3.1	9	4560–5680	m58904a
1992 Oct 16	2448911	A	5.0 × 7.6	90	3.1	9	4520–5680	m58911a
1992 Oct 23	2448918	A	5.0 × 7.6	90	2.4	9	4590–5750	m58918a
1992 Nov 3	2448929	A	5.0 × 7.6	90	3.5	9	4500–5670	m58929a
1992 Nov 27	2448954	A	5.0 × 7.6	90	2.5	9	4550–5710	m58954a
1993 Apr 2	2449079	A	5.0 × 7.6	90	3.2	9	4500–5670	m59079a
1993 Apr 22	2449099	A	5.0 × 7.6	90	3.6	9	4570–5720	m59099a
1993 Apr 30	2449107	A	5.0 × 7.6	90	4.0	9	4510–5660	m59107a
1993 May 7	2449114	A	5.0 × 7.6	90	3.5	9	4470–5630	m59114a
1993 May 21	2449128	A	5.0 × 7.6	90	3.4	9	4530–5660	m59128a
1993 May 28	2449135	A	5.0 × 7.6	90	3.5	9	4510–5660	m59135a
1993 Jun 4	2449142	A	5.0 × 7.6	90	3.2	9	4500–5650	m59142a
1993 Jun 11	2449149	A	5.0 × 7.6	90	4.0	9	4500–5660	m59149a
1993 Jun 18	2449156	A	5.0 × 7.6	90	3.6	9	4530–5690	m59156a
1993 Jun 25	2449163	A	5.0 × 7.6	90	3.0	9	4530–5680	m59163a
1993 Jul 1	2449169	A	5.0 × 7.6	90	2.6	9	4530–5680	m59169a
1993 Jul 8	2449176	A	5.0 × 7.6	90	3.1	9	4530–5690	m59176a
1993 Jul 15	2449183	A	5.0 × 7.6	90	2.6	9	4540–5700	m59183a

TABLE 1—*Continued*

UT Date (1)	Julian Date (2)	Code (3)	Aperture Size (arcsecond) (4)	Aperture P.A. (degree) (5)	Seeing (arcsecond) (6)	Resolution (Å) (7)	Range (Å) (8)	IRAF File (9)
1993 Jul 22	2449190	A	5.0 × 7.6	90	2.4	9	4560–5720	m59190a
1993 Jul 29	2449197	A	5.0 × 7.6	90	3.8	9	4530–5690	m59197a
1993 Aug 6	2449205	A	5.0 × 7.6	90	3.0	9	4540–5700	m59205a
1993 Aug 12	2449211	A	5.0 × 7.6	90	2.9	9	4520–5680	m59211a
1993 Sep 3	2449233	A	5.0 × 7.6	90	2.2	9	4520–5690	m59233a
1993 Sep 10	2449240	A	5.0 × 7.6	90	2.0	9	4530–5690	m59240a
1993 Sep 15	2449245	A	5.0 × 7.6	90	3.1	9	4530–5690	m59245a
1993 Sep 16	2449246	A	5.0 × 7.6	90	2.3	9	4530–5690	m59246a
1993 Sep 23	2449253	A	5.0 × 7.6	90	2.6	9	4520–5670	m59253a
1993 Sep 30	2449260	A	5.0 × 7.6	90	2.8	9	4520–5670	m59260a
1993 Oct 8.....	2449268	A	5.0 × 7.6	90	2.5	9	4520–5670	m59268a
1993 Oct 15	2449275	A	5.0 × 7.6	90	2.2	9	4540–5690	m59275a
1993 Oct 22	2449282	A	5.0 × 7.6	90	2.9	9	4520–5670	m59282a
1993 Nov 5	2449296	A	5.0 × 7.6	90	2.4	9	4530–5690	m59296a
1993 Nov 18.....	2449309	A	5.0 × 7.6	90	2.9	9	4560–5710	m59309a
1993 Nov 25.....	2449316	A	5.0 × 7.6	90	4.1	9	4540–5680	m59316a
1993 Dec 2	2449323	A	5.0 × 7.6	90	3.2	9	4540–5700	m59323a

Note.—Codes for data origin: A, 1.8 m Perkins Telescope + Ohio State CCD Spectrograph; B, 1.6 m Mount Hopkins Telescope + Reticon scanner; C, 5.0 m Hale Telescope + Double Spectrograph; D, 3.0 m Shane Telescope + UV Schmidt Spectrograph; E, 2.3 m Steward Observatory Telescope + CCD Spectrograph; F, 2.2 m Calar Alto Telescope + CCD Spectrograph.

the value given for the seeing is the FWHM of the broad Hβ profile in the cross-dispersion direction; since the BLR is spatially unresolved, the cross-dispersion width is determined by the point-spread function and guiding errors. The rather large values reported here are due primarily to the large zenith distances at which most of the observations were made, and the marked improvement in the mean values in late 1990 is attributable to implementation of an autoguiding system at the telescope (see Peterson et al. 1995 for a more complete description). The nominal spectral resolution and approximate spectral range covered by the data are given in columns (7) and (8), respectively. Finally,

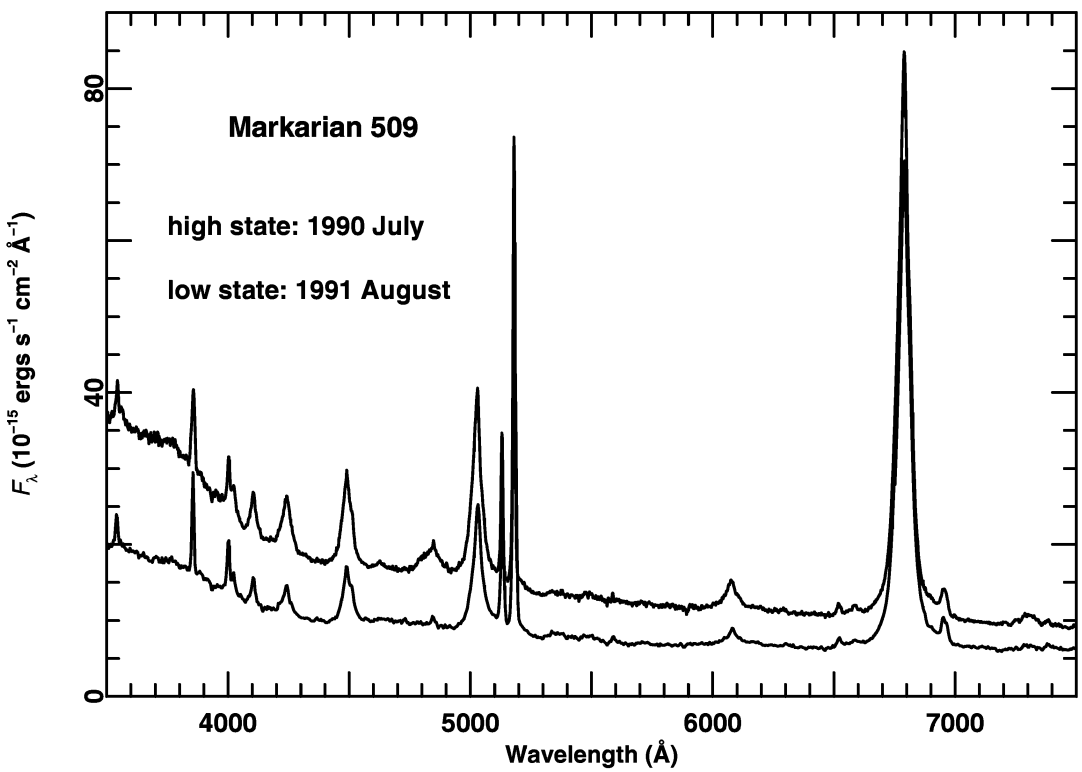

Fig. 1.—Two optical spectra, both obtained with the Lick 3 m Shane telescope, showing high and low states of Mrk 509. The upper spectrum was obtained on JD 2,448,102 (1990 July 30). The lower spectrum was obtained almost exactly 1 year later on JD 2,448,472 (1991 August 4). Fluxes are in units of 10^{-15} ergs s^{-1} cm^{-2} Å^{-1} and are shown in the observed frame. The dramatic variation in the strength of He II λ4686 (just shortward of 5000 Å in the observed frame) is apparent.

to aid future investigators who will make use of these data, column (9) gives a unique identifier by which the spectrum is known to the IRAF reduction system, and which is contained in the FITS file header. The file naming convention is the same as used in our other papers (e.g., Peterson et al. 1991, 1992, 1994; Dietrich et al. 1993; Korista et al. 1995): the first two characters ("m5") identify the galaxy as Mrk 509, and the next four characters (e.g., "7415") contain the four least significant figures in the Julian date, as in column (2). The next character gives the origin of the data, as in column (3), and when necessary, an additional arbitrary character is added to eliminate any remaining ambiguity.

In Figure 1, two sample spectra of Mrk 509 that cover nearly the entire optical spectrum are shown. These spectra were taken at representative high and low flux states, and span the range of activity observed during this 5 year program.

3. ANALYSIS OF THE DATA

In this contribution, we will restrict our attention to measuring the variations of the optical continuum at $\sim$5110 Å and the broad Hβ and He II λ4686 emission lines.

3.1. *Calibration of the Spectra*

Flux calibration of the spectra is accomplished by assuming that the narrow emission lines in the spectra do not vary on the timescales of interest in this experiment. Since these lines arise in a spatially extended ($r \gtrsim 100$ pc) low-density ($n_e \approx 10^3$ cm^{-3}) region, the long light-travel time and recombination time will damp out any variations on timescales as short as a few years. We can therefore measure the flux in the strong narrow lines in each spectrum and multiply each spectrum by a suitable constant that will give the correct integrated flux in the narrow lines. We use the differencing method of van Groningen & Wanders (1992) to obtain the correct multiplicative scaling factor for each spectrum. In this method, one high-quality spectrum is adopted as a reference spectrum (in this case spectrum m58862a). All other spectra are calibrated relative to it by minimizing the residuals of the [O III] $\lambda\lambda$4959, 5007 lines in the difference spectrum produced by subtracting the reference spectrum from a modified version of the spectrum. The narrow-line residuals are minimized in a least-squares fashion by adjusting the multiplicative constant (to adjust the flux scale), the wavelength scale (to account for slight linear wavelength shifts relative to the reference spectrum), and a Gaussian smoothing parameter (which smooths the higher resolution of the two spectra in order to account for slight differences in spectral resolution). By comparing the differences in the optical continuum and emission-line fluxes between closely spaced observations, we estimate that this procedure results in relative errors at the 2%–3% level. With the exception of a few outliers that are the result of observations made under very poor observing conditions, the flux scaling factors are found to be symmetrically distributed about the mean [O III] flux, with a standard deviation of order 15% or so, which reflects the typical accuracy that can be achieved by using standard spectrophotometric flux-calibration techniques.

Absolute calibration of the spectra is accomplished by determining the absolute [O III] λ5007 flux, which is measured from high-quality spectra obtained under photometric conditions through large spectrograph entrance apertures. The absolute [O III] λ5007 fluxes measured from suitable spectra are given in Table 2, and we adopt as our standard the mean of these measurements, F([O III] λ5007) = 6.79×10^{-13} ergs s^{-1} cm^{-2}, as measured in the observed frame.

3.2. *Spectral Measurements*

Continuum and emission-line measurements of the calibrated spectra were made in the following way: the continuum flux was measured at the local minimum in the spectrum immediately longward of Hβ by averaging the flux between 5280 and 5300 Å in the observed frame (i.e., at $\sim$5110 Å in the rest frame of Mrk 509). To measure the Hβ feature, we define a pseudocontinuum by linear interpolation between the fluxes at 4925 and 5280 Å and then integrating the flux above this line between 4930 and 5106 Å (all wavelengths are given in the observed frame). The optical Fe II blends longward and shortward of Hβ are relatively weak in Mrk 509, which also enables us to measure the He II λ4686 flux in a straightforward manner. In this case, we define the pseudocontinuum points at 4750 and 4900 Å and integrate all the flux above this continuum. It was not possible to measure the He II λ4686 feature in those spectra that do not extend to the short wavelength limit of the line integration, which is why there are fewer He II λ4686 measurements than continuum and Hβ measurements. The measurements made from the calibrated spectra are given in Table 3, grouped by common origin as designated by the codes in Table 1. Partial blending of the Hβ and He II λ4686 features is apparent in the brighter states. In principle, our method of setting the pseudocontinuum will thus slightly underestimate the fluxes in both lines. However, the restricted wavelength range of much of the data precludes using a continuum based on more widely separated points. Moreover, the time series analysis that is the most important goal of this investigation is most sensitive to changes in the first and second derivatives of the light curves which are hardly affected at all by precisely how the lines are measured.

3.3. *Intercalibration of the Data*

The individual data sets in Table 3 show similar patterns of variability in both the continuum and the emission lines. However, the light curves produced from the individual sets are slightly offset in flux from one another, and this is attrib-

TABLE 2

ABSOLUTE CALIBRATION

F([O III] λ5007)[a] (1)	File Name (2)
6.47	m57704ea
6.56	m57778ea
6.54	m57779ea
6.25	m57779eb
7.12	m57837a
7.07	m57852a
7.18	m58090a
7.49	m58102d
6.21	m58161d
7.02	m58187a
7.11	m58223c
6.44	m58516a
6.82	m58862a
6.79 $\pm$ 0.40	Mean value

[a] In units of 10^{-13} ergs cm^{-2} s^{-1}.

TABLE 3

MEASUREMENTS OF SPECTRA

Julian Date (1)	F_λ(5110 Å)[a] (2)	F(Hβ)[b] (3)	F(He II)[b] (4)	IRAF File (5)
A. Ohio State CCD				
2447653.....	11.59	12.63	2.16	m57653a
2447657.....	11.86	12.61	1.80	m57657a
2447678.....	11.23	12.34	2.32	m57678a
2447783.....	7.88	11.35	0.54	m57783a
2447788.....	8.44	11.05	0.36	m57788a
2447816.....	9.33	11.28	1.39	m57816a
2447831.....	8.96	10.52	0.92	m57831a
2447837.....	8.95	10.59	0.73	m57837a
2447846.....	9.36	10.62	0.56	m57846a
2447852.....	9.82	10.63	0.41	m57852a
2447868.....	11.75	10.61	1.04	m57868a
2448020.....	12.14	13.43	2.05	m58020a
2448037.....	12.45	12.65	1.44	m58037a
2448044.....	12.47	12.63	1.11	m58044a
2448061.....	13.71	12.31	1.39	m58061a
2448068.....	13.81	12.13	1.83	m58068a
2448077.....	13.93	11.66	1.91	m58077a
2448090.....	13.91	12.04	2.11	m58090a
2448112.....	14.47	12.43	2.81	m58112a
2448128.....	13.57	13.20	2.09	m58128a
2448143.....	13.35	12.80	2.07	m58143a
2448148.....	13.63	13.19	2.24	m58148a
2448149.....	13.83	13.18	1.76	m58149a
2448151.....	14.12	13.26	2.25	m58151a
2448160.....	13.64	12.24	2.29	m58160a
2448175.....	13.12	13.03	2.37	m58175a
2448179.....	12.78	13.18	2.08	m58179a
2448187.....	12.40	13.49	1.86	m58187a
2448193.....	12.32	13.52	1.73	m58193a
2448200.....	12.22	13.30	1.85	m58200a
2448207.....	12.36	13.08	1.80	m58207a
2448220.....	11.64	13.55	1.82	m58220a
2448230.....	10.89	13.65	1.46	m58230a
2448236.....	9.97	13.79	1.48	m58236a
2448421.....	7.08	9.46	0.43	m58421a
2448431.....	6.86	9.00	0.48	m58431a
2448456.....	7.23	8.23	0.18	m58456a
2448460.....	7.41	8.09	0.20	m58460a
2448512.....	9.64	9.02	0.79	m58512a
2448513.....	9.52	8.80	0.85	m58513a
2448514.....	9.38	8.90	0.68	m58514a
2448516.....	9.42	9.16	0.96	m58516a
2448520.....	9.04	8.47	0.99	m58520a
2448534.....	9.56	9.29	0.48	m58534a
2448733.....	10.39	11.06	0.45	m58733a
2448780.....	12.90	12.13	1.14	m58780a
2448789.....	12.82	12.90	1.43	m58789a
2448796.....	12.69	12.51	1.05	m58796a
2448810.....	13.68	12.50	1.03	m58810a
2448817.....	14.62	12.82	1.51	m58817a
2448825.....	14.61	12.63	1.72	m58825a
2448839.....	14.38	12.81	1.39	m58839a
2448848.....	14.61	13.64	1.59	m58848a
2448862.....	14.26	13.47	1.84	m58862a
2448869.....	14.39	13.36	1.83	m58869a
2448876.....	14.76	13.42	1.74	m58876a
2448883.....	14.65	13.66	2.00	m58883a
2448889.....	14.38	13.68	1.94	m58889a
2448898.....	14.42	13.76	1.94	m58898a
2448904.....	14.27	14.12	2.01	m58904a
2448911.....	14.47	14.38	2.07	m58911a
2448918.....	13.79	13.64	1.65	m58918a
2448929.....	14.08	13.61	1.91	m58929a
2448954.....	14.07	14.66	1.74	m58954a
2449079.....	12.51	13.84	2.33	m59079a
2449099.....	11.58	13.72	2.23	m59099a
2449107.....	10.97	13.90	2.23	m59107a
2449114.....	10.29	14.29	1.73	m59114a

TABLE 3—*Continued*

Julian Date (1)	F_λ(5110 Å)[a] (2)	F(Hβ)[b] (3)	F(He II)[b] (4)	IRAF File (5)
2449128.....	10.33	13.61	1.84	m59128a
2449135.....	10.29	13.94	1.85	m59135a
2449142.....	10.14	13.70	1.99	m59142a
2449149.....	10.04	13.77	2.12	m59149a
2449156.....	9.80	13.16	1.90	m59156a
2449163.....	9.25	13.36	1.62	m59163a
2449169.....	8.92	13.30	1.31	m59169a
2449176.....	8.67	12.96	1.23	m59176a
2449183.....	8.60	12.72	1.04	m59183a
2449190.....	9.21	12.14	1.11	m59190a
2449197.....	9.60	11.88	1.47	m59197a
2449205.....	9.77	11.82	1.83	m59205a
2449211.....	9.73	12.16	1.78	m59211a
2449233.....	9.53	12.18	1.72	m59233a
2449240.....	9.17	12.00	1.47	m59240a
2449245.....	9.05	12.04	1.44	m59245a
2449246.....	8.96	12.16	1.36	m59246a
2449253.....	9.09	12.02	1.29	m59253a
2449260.....	9.10	12.11	1.07	m59260a
2449268.....	9.54	11.68	1.46	m59268a
2449275.....	9.44	11.67	1.50	m59275a
2449282.....	9.66	12.50	1.70	m59282a
2449296.....	9.42	11.81	1.46	m59296a
2449309.....	9.89	11.76	1.48	m59309a
2449316.....	9.76	11.83	1.92	m59316a
2449323.....	9.59	11.78	1.78	m59323a
B. SAO Reticon				
2447415.....	10.94	13.42	...	m57415b
2447420.....	10.76	13.18	...	m57420b
2447421.....	10.52	13.39	...	m57421b
2447442.....	11.26	12.77	...	m57442b
2447446.....	10.72	12.82	...	m57446b
2447472.....	10.98	13.40	...	m57472b
2447478.....	10.85	13.23	...	m57478b
2447497.....	11.02	13.51	...	m57497b
2447498.....	11.46	14.35	...	m57498b
2447500.....	10.96	13.57	...	m57500b
2447501.....	11.12	15.13	...	m57501b
2447717.....	11.50	15.78	...	m57717b
2447777.....	8.06	13.79	...	m57777b
2447798.....	9.31	14.46	...	m57798b
2447799.....	9.23	13.81	...	m57799b
2447800.....	9.23	13.57	...	m57800b
2447805.....	9.30	13.19	...	m57805b
2447823.....	9.49	13.09	...	m57823b
2447824.....	10.01	12.09	...	m57824b
2447826.....	9.68	13.47	...	m57826b
2447829.....	9.04	13.34	...	m57829b
2447831.....	8.71	12.62	...	m57831b
2447832.....	8.91	12.90	...	m57832b
2447833.....	8.83	13.28	...	m57833b
2447834.....	8.63	12.48	...	m57834b
2447835.....	8.49	12.19	...	m57835b
2447859.....	11.17	12.81	...	m57859b
2448059.....	12.92	14.93	...	m58059b
2448060.....	12.59	13.58	...	m58060b
2448061.....	12.31	14.55	...	m58061b
2448064.....	13.42	13.79	...	m58064b
2448065.....	13.23	15.10	...	m58065b
2448151.....	13.71	14.58	...	m58151b
2448162.....	13.72	14.65	...	m58162b
2448179.....	13.54	16.54	...	m58179b
2448187.....	12.99	16.75	...	m58187b
2448188.....	12.08	16.28	...	m58188b
2448189.....	12.30	14.72	...	m58189b
C. Palomar Double Spectrograph				
2448223.....	10.35	13.96	2.49	m58223c

TABLE 3—*Continued*

Julian Date (1)	F_λ(5110 Å)[a] (2)	F(Hβ)[b] (3)	F(He II)[b] (4)	IRAF File (5)
D. Lick Shane CCD				
2448102....	14.34	12.88	2.20	m58102d
2448161....	14.53	13.33	2.60	m58161d
2448184....	14.24	15.02	1.73	m58184d
2448206....	13.78	14.96	1.80	m58206d
2448472....	7.96	9.14	0.41	m58472d
2448487....	9.30	9.35	0.39	m58487d
2448798....	13.15	13.51	1.33	m58798d
E. Steward CCD				
2447704....	11.77	13.65	2.28	m57704ea
2447767....	9.22	12.74	1.15	m57767ea
2447778....	8.57	12.38	0.51	m57778ea
2447779....	8.68	11.58	0.73	m57779ea
F. Calar Alto CCD				
2447663....	11.57	13.43	2.91	m57663fa
2447664....	11.60	14.02	3.11	m57664fa
2447826....	8.97	11.90	1.50	m57826f
2448088....	13.34	13.53	2.32	m58088f

[a] In units of 10^{-15} ergs s^{-1} cm^{-2} Å^{-1}.
[b] In units of 10^{-13} ergs s^{-1} cm^{-2}.

uted to aperture effects. As in our other papers (Peterson et al. 1991, 1992, 1994; Dietrich et al. 1993; Korista et al. 1995), we determine an empirical correction for each of the data sets to bring them on to a common flux scale. We do this by arbitrarily adopting the largest data set (set "A") as a standard, and applying corrections to the other sets to bring measurements from the various sources into agreement. We first define a point-source correction factor φ by the equation

$$F(\mathrm{H}\beta) = \varphi F(\mathrm{H}\beta)_{\rm obs} , \qquad (2)$$

where the observed Hβ fluxes $F(\mathrm{H}\beta)_{\rm obs}$ are as given in Table 3. This factor accounts for the fact that different apertures result in different amounts of light loss for the point-spread function (which describes the surface-brightness distribution of both the broad lines and the AGN continuum source) and the partially extended narrow-line region. We note, of course, that this correction factor is in principle a function of seeing (Peterson et al. 1995). We do not attempt to correct for seeing effects, and thus seeing effects probably contribute much of the total uncertainty in the measurements.

After applying the point-spread function correction φ, another correction needs to be applied to adjust for the different amounts of starlight admitted by different apertures. We define an extended source correction G as

$$F_\lambda(5100\ \text{Å}) = \varphi F_\lambda(5100\ \text{Å})_{\rm obs} - G , \qquad (3)$$

where again $F_\lambda(5100\ \text{Å})_{\rm obs}$ is from Table 3. The process of intercalibrating the various data sets is then carried out by comparing pairs of nearly simultaneous observations (i.e., to within 4 days) from different data sets to determine for each data set the values of the constants φ and G that are needed to adjust the emission-line and continuum fluxes to a common scale. Furthermore, the formal uncertainties in φ and G reflect the uncertainties in the individual data sets, so we can determine the nominal uncertainties for each data set if we assume that the errors add in quadrature. For the larger data sets, fractional uncertainties can be estimated independently by comparing closely spaced measurements. For the various data sets we find typical uncertainties of ~2%–3% in the continuum and Hβ fluxes and ~13% in He II λ4686.

TABLE 4

FLUX SCALE FACTORS

Data Set (1)	Point-Source Scale Factor ϕ (2)	Extended Source Correction G[a] (3)
A.....	1.000	0.000
B.....	0.843 ± 0.042	−1.952 ± 0.058
C.....	0.970	−1.590
D.....	0.904 ± 0.023	−0.175 ± 0.576
E.....	0.980	0.636
F.....	0.905 ± 0.039	−1.501 ± 0.345

[a] In units of 10^{-15} ergs s^{-1} cm^{-2} Å^{-1}.

The intercalibration constants we use for each data set are given in Table 4, and these constants are used with equations (2) and (3) to adjust the measurements given in Table 3 to a common flux scale, which corresponds to measurements through the 5″.0 × 7″.5 spectrograph entrance aperture used in set "A." The resultant values of the continuum flux F_λ(5100 Å) and the line fluxes F(Hβ) and F(He II λ4686) are given in Table 5, which gives the complete light curve produced by computing the variance-weighted average of all the adjusted measurements obtained on a given Julian date. After completing the intercalibration, we can perform an additional check of our error estimates by examining the ratios of all pairs of closely spaced points in Table 5. In Table 5, there are 72 pairs of continuum measurements separated by 4 days or less, and we compute the ratio of all such pairs of measurements. The dispersion about the mean value of unity, divided by $2^{1/2}$, provides an estimate of the typical uncertainty in a single measurement. For the continuum, we find that the mean fractional error in a given measurement is 0.029. The average fractional uncertainty, from the quoted estimates for these same 72 measurements in Table 5, is 0.025, which implies that our error estimates are probably quite good. A similar analysis of the Hβ fluxes (again with 72 pairs separated by 4 days or less) yields an estimated uncertainty of 0.034, compared to the mean quoted error of 0.028, and for He II λ4686 (with 23 pairs of closely spaced points), the uncertainty estimated from the dispersion in the ratios of closely spaced measurements is 0.13, which is identical to the mean quoted error.

4. VARIABILITY ANALYSIS

4.1. *Characteristics of the Data Base*

Figure 2 shows the 5110 Å continuum and Hβ and He II λ4686 emission-line light curves from Table 5. The continuum and Hβ measurements span a total of 1909 days, and the He II λ4686 data cover 1671 days. Inspection of Figure 2 shows that the continuum and emission lines underwent large variations during the monitoring period and that in general these variations appear to be smooth and quite slow, at least in comparison to those seen in other well studied sources such as NGC 4151 (Clavel et al. 1990; Ulrich et al. 1991; Crenshaw et al. 1996), NGC 5548 (Peterson et al. 1994, and references therein), and NGC 3783 (Reichert et al. 1994; Stirpe et al. 1994). The variations

TABLE 5

OPTICAL CONTINUUM AND EMISSION-LINE LIGHT CURVES

Julian Date (1)	F_λ(5110 Å)[a] (2)	F(Hβ)[b] (3)	F(He II)[b] (4)
2447415.....	11.17 ± 0.62	11.31 ± 0.45	...
2447420.....	11.03 ± 0.61	11.11 ± 0.44	...
2447421.....	10.82 ± 0.60	11.29 ± 0.45	...
2447442.....	11.44 ± 0.63	10.76 ± 0.43	...
2447446.....	10.99 ± 0.60	10.81 ± 0.43	...
2447472.....	11.21 ± 0.62	11.30 ± 0.45	...
2447478.....	11.10 ± 0.61	11.15 ± 0.45	...
2447497.....	11.24 ± 0.62	11.39 ± 0.46	...
2447498.....	11.61 ± 0.64	12.10 ± 0.48	...
2447500.....	11.19 ± 0.62	11.44 ± 0.46	...
2447501.....	11.32 ± 0.62	12.76 ± 0.51	...
2447653.....	11.59 ± 0.23	12.63 ± 0.32	2.16 ± 0.28
2447657.....	11.86 ± 0.24	12.61 ± 0.31	1.80 ± 0.23
2447663.....	11.97 ± 0.30	12.15 ± 0.30	2.63 ± 0.34
2447664.....	12.00 ± 0.30	12.69 ± 0.32	2.82 ± 0.37
2447678.....	11.23 ± 0.22	12.34 ± 0.31	2.32 ± 0.30
2447704.....	10.90 ± 0.33	13.37 ± 0.33	2.24 ± 0.29
2447717.....	11.65 ± 0.64	13.30 ± 0.53	...
2447767.....	8.40 ± 0.25	12.48 ± 0.31	1.13 ± 0.15
2447777.....	8.75 ± 0.48	11.62 ± 0.47	...
2447778.....	7.77 ± 0.23	12.14 ± 0.30	0.50 ± 0.06
2447779.....	7.87 ± 0.24	11.35 ± 0.28	0.71 ± 0.09
2447783.....	7.88 ± 0.16	11.35 ± 0.28	0.54 ± 0.07
2447788.....	8.44 ± 0.17	11.05 ± 0.28	0.36 ± 0.05
2447798.....	9.80 ± 0.54	12.19 ± 0.49	...
2447799.....	9.73 ± 0.54	11.65 ± 0.47	...
2447800.....	9.73 ± 0.54	11.44 ± 0.46	...
2447805.....	9.79 ± 0.54	11.12 ± 0.44	...
2447816.....	9.33 ± 0.19	11.28 ± 0.28	1.39 ± 0.18
2447823.....	9.95 ± 0.55	11.03 ± 0.44	...
2447824.....	10.39 ± 0.57	10.19 ± 0.41	...
2447826.....	9.70 ± 0.22	10.92 ± 0.23	1.36 ± 0.18
2447829.....	9.57 ± 0.53	11.25 ± 0.45	...
2447831.....	9.00 ± 0.17	10.55 ± 0.22	0.92 ± 0.12
2447832.....	9.47 ± 0.52	10.88 ± 0.44	...
2447833.....	9.40 ± 0.52	11.19 ± 0.45	...
2447834.....	9.23 ± 0.51	10.52 ± 0.42	...
2447835.....	9.11 ± 0.50	10.27 ± 0.41	...
2447837.....	8.95 ± 0.18	10.59 ± 0.26	0.73 ± 0.09
2447846.....	9.36 ± 0.19	10.62 ± 0.27	0.56 ± 0.07
2447852.....	9.82 ± 0.20	10.63 ± 0.27	0.41 ± 0.05
2447859.....	11.37 ± 0.62	10.80 ± 0.43	...
2447868.....	11.75 ± 0.23	10.61 ± 0.26	1.04 ± 0.14
2448020.....	12.14 ± 0.24	13.43 ± 0.34	2.05 ± 0.27
2448037.....	12.45 ± 0.25	12.65 ± 0.32	1.44 ± 0.19
2448044.....	12.47 ± 0.25	12.63 ± 0.32	1.11 ± 0.14
2448059.....	12.84 ± 0.71	12.59 ± 0.50	...
2448060.....	12.56 ± 0.69	11.45 ± 0.46	...
2448061.....	13.52 ± 0.25	12.29 ± 0.26	1.39 ± 0.18
2448064.....	13.26 ± 0.73	11.63 ± 0.47	...
2448065.....	13.10 ± 0.72	12.73 ± 0.51	...
2448068.....	13.81 ± 0.28	12.13 ± 0.30	1.83 ± 0.24
2448077.....	13.93 ± 0.28	11.66 ± 0.29	1.91 ± 0.25
2448088.....	13.57 ± 0.34	12.24 ± 0.31	2.10 ± 0.27
2448090.....	13.91 ± 0.28	12.04 ± 0.30	2.11 ± 0.28
2448102.....	13.14 ± 0.39	11.64 ± 0.29	1.99 ± 0.26
2448112.....	14.47 ± 0.29	12.43 ± 0.31	2.81 ± 0.37
2448128.....	13.57 ± 0.27	13.20 ± 0.33	2.09 ± 0.27
2448143.....	13.35 ± 0.27	12.80 ± 0.32	2.07 ± 0.27
2448148.....	13.63 ± 0.27	13.19 ± 0.33	2.24 ± 0.29
2448149.....	13.83 ± 0.28	13.18 ± 0.33	1.76 ± 0.23
2448151.....	14.04 ± 0.26	12.95 ± 0.27	2.25 ± 0.29
2448160.....	13.64 ± 0.27	12.24 ± 0.31	2.29 ± 0.30
2448161.....	13.31 ± 0.40	12.05 ± 0.30	2.35 ± 0.31
2448162.....	13.52 ± 0.74	12.35 ± 0.49	...
2448175.....	13.12 ± 0.26	13.03 ± 0.33	2.37 ± 0.31
2448179.....	12.85 ± 0.24	13.38 ± 0.28	2.08 ± 0.27
2448184.....	13.05 ± 0.39	13.58 ± 0.34	1.57 ± 0.20
2448187.....	12.45 ± 0.23	13.66 ± 0.29	1.86 ± 0.24
2448188.....	12.14 ± 0.67	13.72 ± 0.55	...
2448189.....	12.32 ± 0.68	12.41 ± 0.50	...
2448193.....	12.32 ± 0.25	13.52 ± 0.34	1.73 ± 0.22
2448200.....	12.22 ± 0.24	13.30 ± 0.33	1.85 ± 0.24
2448206.....	12.63 ± 0.38	13.52 ± 0.34	1.63 ± 0.21
2448207.....	12.36 ± 0.25	13.08 ± 0.33	1.80 ± 0.23
2448220.....	11.64 ± 0.23	13.55 ± 0.34	1.82 ± 0.24
2448223.....	11.63 ± 0.35	13.54 ± 0.34	2.41 ± 0.31
2448230.....	10.89 ± 0.22	13.65 ± 0.34	1.46 ± 0.19
2448236.....	9.97 ± 0.20	13.79 ± 0.34	1.48 ± 0.19
2448421.....	7.08 ± 0.14	9.46 ± 0.24	0.43 ± 0.06
2448431.....	6.86 ± 0.14	9.00 ± 0.22	0.48 ± 0.06
2448456.....	7.23 ± 0.14	8.23 ± 0.21	0.18 ± 0.02
2448460.....	7.41 ± 0.15	8.09 ± 0.20	0.20 ± 0.03
2448472.....	7.37 ± 0.22	8.27 ± 0.21	0.38 ± 0.05
2448487.....	8.59 ± 0.26	8.45 ± 0.21	0.36 ± 0.05
2448512.....	9.64 ± 0.19	9.02 ± 0.22	0.79 ± 0.10
2448513.....	9.52 ± 0.19	8.80 ± 0.22	0.85 ± 0.11
2448514.....	9.38 ± 0.19	8.90 ± 0.22	0.68 ± 0.09
2448516.....	9.42 ± 0.19	9.16 ± 0.23	0.96 ± 0.12
2448520.....	9.04 ± 0.18	8.47 ± 0.21	0.99 ± 0.13
2448534.....	9.56 ± 0.19	9.29 ± 0.23	0.48 ± 0.06
2448733.....	10.39 ± 0.21	11.06 ± 0.28	0.45 ± 0.06
2448780.....	12.90 ± 0.26	12.13 ± 0.30	1.14 ± 0.15
2448789.....	12.82 ± 0.26	12.90 ± 0.32	1.43 ± 0.19
2448796.....	12.69 ± 0.25	12.51 ± 0.31	1.05 ± 0.14
2448798.....	12.07 ± 0.36	12.21 ± 0.31	1.20 ± 0.16
2448810.....	13.68 ± 0.27	12.50 ± 0.31	1.03 ± 0.13
2448817.....	14.62 ± 0.29	12.82 ± 0.32	1.51 ± 0.20
2448825.....	14.61 ± 0.29	12.63 ± 0.32	1.72 ± 0.22
2448839.....	14.38 ± 0.29	12.81 ± 0.32	1.39 ± 0.18
2448848.....	14.61 ± 0.29	13.64 ± 0.34	1.59 ± 0.21
2448862.....	14.26 ± 0.28	13.47 ± 0.34	1.84 ± 0.24
2448869.....	14.39 ± 0.29	13.36 ± 0.33	1.83 ± 0.24
2448876.....	14.76 ± 0.29	13.42 ± 0.34	1.74 ± 0.23
2448883.....	14.65 ± 0.29	13.66 ± 0.34	2.00 ± 0.26
2448889.....	14.38 ± 0.29	13.68 ± 0.34	1.94 ± 0.25
2448898.....	14.42 ± 0.29	13.76 ± 0.34	1.94 ± 0.25
2448904.....	14.27 ± 0.28	14.12 ± 0.35	2.01 ± 0.26
2448911.....	14.47 ± 0.29	14.38 ± 0.36	2.07 ± 0.27
2448918.....	13.79 ± 0.28	13.64 ± 0.34	1.65 ± 0.22
2448929.....	14.08 ± 0.28	13.61 ± 0.34	1.91 ± 0.25
2448954.....	14.07 ± 0.28	14.66 ± 0.37	1.74 ± 0.23
2449079.....	12.51 ± 0.25	13.84 ± 0.35	2.33 ± 0.30
2449099.....	11.58 ± 0.23	13.72 ± 0.34	2.23 ± 0.29
2449107.....	10.97 ± 0.22	13.90 ± 0.35	2.23 ± 0.29
2449114.....	10.29 ± 0.21	14.29 ± 0.36	1.73 ± 0.22
2449128.....	10.33 ± 0.21	13.61 ± 0.34	1.84 ± 0.24
2449135.....	10.19 ± 0.20	13.94 ± 0.35	1.85 ± 0.24
2449142.....	10.14 ± 0.20	13.70 ± 0.34	1.99 ± 0.26
2449149.....	10.04 ± 0.20	13.77 ± 0.34	2.12 ± 0.28
2449156.....	9.80 ± 0.20	13.16 ± 0.33	1.90 ± 0.25
2449163.....	9.25 ± 0.19	13.36 ± 0.33	1.62 ± 0.21
2449169.....	8.92 ± 0.18	13.30 ± 0.33	1.31 ± 0.17
2449176.....	8.67 ± 0.17	12.96 ± 0.32	1.23 ± 0.16
2449183.....	8.60 ± 0.17	12.72 ± 0.32	1.04 ± 0.14
2449190.....	9.21 ± 0.18	12.14 ± 0.30	1.11 ± 0.14
2449197.....	9.60 ± 0.19	11.89 ± 0.30	1.47 ± 0.19
2449205.....	9.77 ± 0.19	11.82 ± 0.29	1.83 ± 0.24
2449211.....	9.74 ± 0.19	12.16 ± 0.30	1.78 ± 0.23
2449233.....	9.53 ± 0.19	12.18 ± 0.31	1.72 ± 0.22
2449240.....	9.17 ± 0.18	12.00 ± 0.30	1.47 ± 0.19
2449245.....	9.05 ± 0.18	12.04 ± 0.30	1.44 ± 0.19
2449246.....	8.96 ± 0.18	12.16 ± 0.30	1.36 ± 0.18
2449253.....	9.09 ± 0.18	12.02 ± 0.30	1.29 ± 0.17
2449260.....	9.10 ± 0.18	12.11 ± 0.30	1.07 ± 0.14
2449268.....	9.54 ± 0.19	11.68 ± 0.29	1.46 ± 0.19
2449275.....	9.44 ± 0.19	11.67 ± 0.29	1.50 ± 0.19
2449282.....	9.66 ± 0.19	12.50 ± 0.31	1.70 ± 0.22
2449296.....	9.41 ± 0.19	11.81 ± 0.29	1.46 ± 0.19
2449309.....	9.89 ± 0.20	11.76 ± 0.29	1.48 ± 0.19
2449316.....	9.76 ± 0.19	11.83 ± 0.30	1.92 ± 0.25
2449323.....	9.59 ± 0.19	11.78 ± 0.29	1.78 ± 0.23

TABLE 5—*Continued*

[a] In units of 10^{-15} ergs s^{-1} cm^{-2} Å^{-1}.

[b] In units of 10^{-13} ergs s^{-1} cm^{-2}.

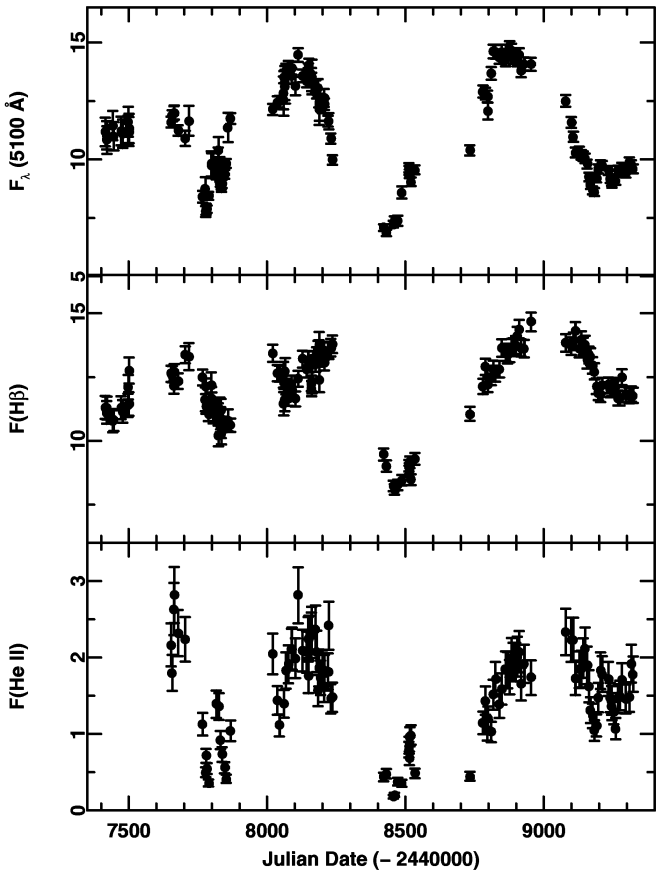

FIG. 2.—The continuum fluxes at 5110 Å (*top panel*), Hβ emission-line fluxes (*middle panel*), and He II λ4686 fluxes (*bottom panel*) for Mrk 509, as given in Table 5, from 1989 September to 1993 December. Fluxes are in the observed frame and are in units of 10^{-15} ergs s^{-1} cm^{-2} Å^{-1} for the continuum and 10^{-13} ergs s^{-1} cm^{-2} for the lines.

appear to be well resolved with our median sampling of 7 days. The relatively large interseason gaps are due to the southern declination ($\delta \approx -11°$) of Mrk 509; all of the telescopes that were employed in this study are at northern hemisphere observatories. These gaps introduce some uncertainty into our conclusions, since in no single observing season did we see the related inflection points in the continuum and Hβ light curves that are required for an unambiguous measurement of the time delay. This bright source would be an excellent candidate for a long-term southern hemisphere monitoring program.

The sampling characteristics of this experiment and some simple parameters that describe the amplitude of variation are given in Table 6. The fractional variation F_{var} is the ratio of the rms fluctuation to the mean flux and is corrected for the effect of measurement errors (see Clavel et al. 1991). The parameter R_{max} is the ratio of maximum to minimum flux. Neither of these parameters has been adjusted for the effects of nonvarying components, such as the stellar continuum or the narrow components of the emission lines.

4.2. *Time Series Analysis*

A characteristic response time for the broad emission lines can be determined by cross-correlation of the continuum and emission-line light curves. We employ both of the commonly used methods for cross-correlation of unevenly sampled AGN light curves, the interpolation method of Gaskell & Sparke (1986) and the discrete correlation function (DCF) method of Edelson & Krolik (1988). The specific versions of the algorithms we use are described by White & Peterson (1994).

The results of the cross-correlation analysis are summarized in Table 7. The correlation functions computed from the entire data sets are shown in Figure 3. The upper panel of Figure 3 shows the interpolation CCF and the DCF obtained by cross-correlation of the optical continuum and Hβ light curves. The middle panel shows the optical continuum/He II λ4686 cross-correlation. The lower panel shows both the corresponding continuum autocorrelation function (ACF) and the sampling window autocorrelation function; the latter is produced by averaging the ACFs obtained by repeatedly sampling a white noise spectrum in exactly the same pattern as the real observations and then computing the ACF by the interpolation method. The interpolation process automatically introduces a correlation extending from zero lag to a value that characterizes the typical sampling interval, and thus the sampling window ACF provides a good indication of how much of the width of the ACF is due to interpolation rather than to real correlation between continuum points at different times (see Gaskell & Peterson 1987). The ACF (FWHM = 191 days) is very much broader than the sampling window ACF (FWHM = 7 days), which indicates that the cross-correlation results are not dominated by interpolation artifacts. In Table 7, the parameter r_{max} is the peak value of the interpolation CCF, which occurs at a time delay τ_{peak}, and τ_{cent} refers to the centroid of the CCF, which is computed by including only those points within $0.5r_{max}$.

In order to assess how robust our calibration and cross-correlation procedures are, we also carried out the time series analysis based on only the single largest data set (set "A"), and these results are also given in Table 7. Only the He II λ4686 centroid changes significantly. That this is due primarily to the omission of the continuum points from the first year (i.e., prior to JD 2,447,653) is demonstrated by again using the full data base, but excluding the more-or-

TABLE 6

VARIABILITY PARAMETERS AND SAMPLING CHARACTERISTICS

FEATURE (1)	NUMBER OF EPOCHS (2)	TOTAL SPAN (DAYS) (3)	SAMPLING INTERVAL (DAYS)		MEAN FLUX[a] (6)	F_{var} (7)	R_{max} (8)
			Average (4)	Median (5)			
F_λ(5110 Å)	142	1909	13.5	7	11.17	0.182	2.15
Hβ λ4861.....	142	1909	13.5	7	12.06	0.119	1.81
He II λ4686.....	110	1671	15.3	7	1.53	0.382	15.8

[a] Units as in Table 5.

TABLE 7

CROSS-CORRELATION RESULTS: OPTICAL CONTINUUM VERSUS EMISSION LINES

	Hβ λ4861			He II λ4686		
DATA SET (1)	τ_{peak} (days) (2)	τ_{cent} (days) (3)	r_{max} (4)	τ_{peak} (days) (5)	τ_{cent} (days) (6)	r_{max} (7)
All data	86	80.2	0.878	64	61.8	0.725
Set A only	87	87.4	0.889	58	87.7	0.738
JD 2447653 – 2449323 only.....	86	81.0	0.882	64	81.3	0.753

less isolated continuum points from the first year (see Table 7); the range in time considered is more important than either the total number of data points or the effects of the intercalibration process.

The cross-correlation lags are well defined quantities, although the results shown in Table 7 make it clear that ambiguities can arise depending the computational details. There is no generally agreed upon way to establish formal uncertainties for lags measured from unevenly sampled data drawn from irregular light curves. Monte Carlo simulations are often employed, but the results are nevertheless very sensitive to the specific model assumptions that are made.

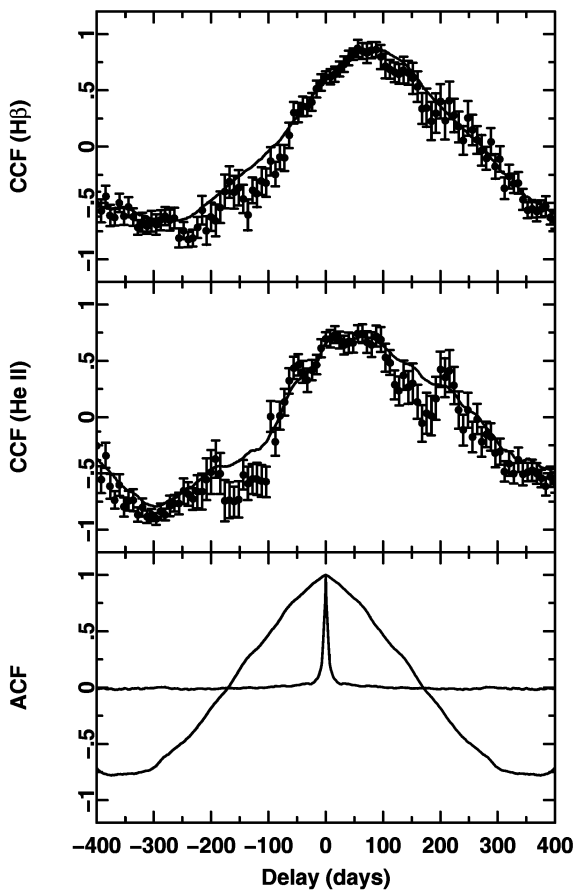

FIG. 3.—The top panel shows the optical continuum–Hβ cross-correlation function computed from the data in Table 5 and Fig. 2. The optical continuum–He II λ4686 cross-correlation function is shown in the middle panel. The solid lines show the interpolation cross-correlation function (Gaskell & Sparke 1986), and the filled circles with error bars show the DCF values (Edelson & Krolik 1988), in both cases computed as described by White & Peterson (1994). The bin width for the DCF is 8 days. The optical continuum autocorrelation function and the sampling window autocorrelation function appear in the lower panel.

Gaskell & Peterson (1987) suggest an analytic formula for estimating the uncertainties in cross-correlation lags. Comparison of estimates based on this formula with results of Monte Carlo simulations suggests that the Gaskell-Peterson formula slightly overestimates the errors when the light curves are well sampled (as they appear to be in this case), but grossly underestimate the errors when the sampling is poor (Maoz & Netzer 1989; White & Peterson 1994). For the CCFs computed here, the Gaskell-Peterson formula yields estimates of the uncertainties in the lags of ~7 days, which is about the same as the median sampling interval. We emphasize that the cross-correlation lag gives merely a scale length for the BLR and that when good sampling is achieved the uncertainties in the BLR geometry become far more important than the formal uncertainties in the cross-correlation lag measurements.

5. DISCUSSION

A striking result of this program is that the emission-line lags are so large and the continuum variations so slow that it would not have been possible to measure the lag accurately based on data from only a single observing season. Indeed, we were somewhat confused by the data from the first 2 years of data because derivatives of the continuum and Hβ light curves seemed to have different signs much of the time, and it was only with several years of data that the true pattern began to emerge.

The lags measured for Hβ and He II λ4686 in Mrk 509 are a factor of 3–4 larger than lags that have been reliably measured for these lines in other AGNs. Only in the case of the very luminous Seyfert 1 galaxy Fairall 9 (Clavel, Wamsteker, & Glass 1989) have longer lags been reliably measured for any lines, and the formal measurement errors are uncomfortably large in that case (see Shields, Ferland, & Peterson 1995). We illustrate this in Figure 4, which shows the relationship between the size of the Balmer-line emitting region (usually based on Hβ lags, but in some cases on Hα) and the optical continuum specific luminosity for well observed AGNs. The data were drawn from published sources, in order of increasing optical luminosity, from Maoz et al. (1991) for NGC 4151, Salamanca et al. (1994) and Winge et al. (1995) for NGC 3227, Dietrich et al. (1994) for NGC 4593, Winge et al. (1996) for IC 4329A, Stirpe et al. (1994) for NGC 3783, Peterson et al. (1994) for NGC 5548, Wanders et al. (1993) for NGC 3516, Peterson et al. (1993) for Mrk 590, Kassebaum et al. (1996) for Mrk 335, Maoz et al. (1990) for Mrk 279, and this paper for Mrk 509. Figure 4 is plotted so that a diagonal line corresponds to the prediction of equation (1). On the basis of the data shown in Figure 4, the prediction of equation (1) is neither verified nor disproved. The fact that a large lag is measured for the most luminous source is of course reassuring, but the range

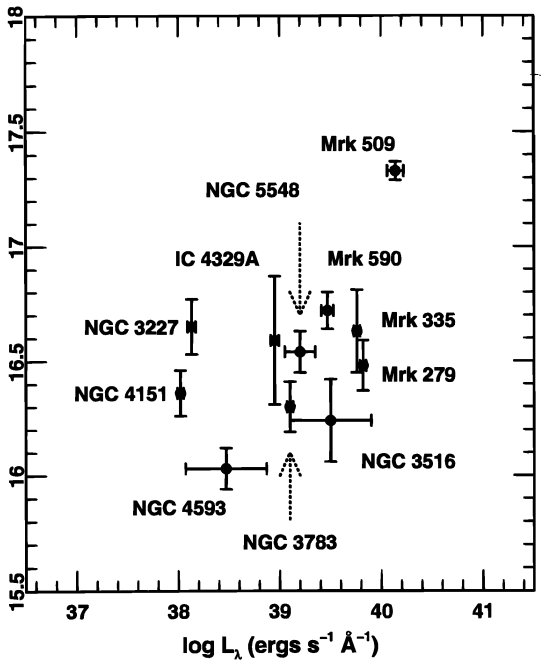

FIG. 4.—The radius-luminosity relationship for the broad-line regions in Seyfert galaxies. The BLR radius is taken to be $r = c\tau_{cent}$, where τ_{cent} is the centroid of the optical continuum/Balmer-line (usually Hβ) cross-correlation function. The optical specific luminosity (for $H_0 = 100$ km s^{-1} Mpc^{-1}) generally refers to the AGN component only, i.e., with the starlight contribution subtracted whenever possible.

of luminosity that has been explored at this time is still not sufficient to adequately test the relationship. There are several sources of widely different luminosities which have very similar Balmer-line lags in the range of two to three weeks (corresponding to BLR scale lengths of ~ 3–5×10^{16} cm), and these introduce much scatter into the observed relationship. This is plausibly attributable to these AGNs having slightly different spectral shapes and emission-line strengths, in which case the $r \propto L^{1/2}$ prediction is so approximate that a larger range of luminosity or more detailed photoionization modeling of individual sources will be required for a meaningful test.

We are very grateful to the Directors and Telescope Allocation Committees of our various observatories for their support of this project. Individual investigators have benefited from support from a number of agencies, including the following: the National Science Foundation: AST 91-17086 and AST 94-20080 (Ohio State University), AST 89-57063 and AST 90-03829 (University of California, Berkeley), and the NSF Graduate Fellowship program (T. M.); NASA: NAG 5-1630 (P. S. S.), NAS 8-30751 and NAS 5-30934 (Center for Astrophysics), and Long-Term Space Astrophysics grant NAGW-3315 (B. M. P.); and BMFT grant Verbundforschung Astronomie DFG Ko857/13-1 (Universitäts-Sternwarte Göttingen).

REFERENCES

Blandford, R. D., & McKee, C. F. 1982, ApJ, 255, 419
Clavel, J., et al. 1990, MNRAS, 246, 668
———. 1991, ApJ, 366, 64
Clavel, J., Wamsteker, W., & Glass, I. S. 1989, ApJ, 337, 236
Crenshaw, D. M., et al. 1996, ApJ, 470, in press
Dietrich, M., et al. 1993, ApJ, 408, 416
———. 1994, A&A, 284, 33
Edelson, R. A., & Krolik, J. H. 1988, ApJ, 333, 646
Erkens, U., et al. 1995, A&A, 296, 90
Gaskell, C. M., & Peterson, B. M., 1987, ApJS, 65, 1
Gaskell, C. M., & Sparke, L. S. 1986, ApJ, 305, 175
Kassebaum, T. M., Peterson, B. M., Wanders, I., Pogge, R. W., Bertram, R., & Wagner, R. M. 1996, ApJ, submitted
Korista, K. T., et al. 1995, ApJS, 97, 285
Maoz, D. 1994, in Reverberation Mapping of the Broad-Line Region in Active Galactic Nuclei, ed. P. M. Gondhalekar, K. Horne, & B. M. Peterson (San Francisco: ASP), 95
Maoz, D., et al. 1990, ApJ, 351, 75
———. 1991, ApJ, 367, 493
Maoz, D., & Netzer, H.. 1989, MNRAS, 236, 21
Maoz, D., Smith, P. S., Jannuzi, B. T., Kaspi, S., & Netzer, H. 1994, ApJ, 421, 34
Peterson, B. M. 1993, PASP, 105, 247
Peterson, B. M. 1994, in Reverberation Mapping of the Broad-Line Region in Active Galactic Nuclei, ed. P. M. Gondhalekar, K. Horne, & B. M. Peterson (San Francisco: ASP), 1
Peterson, B. M., et al. 1991, ApJ, 368, 119
———. 1992, ApJ, 392, 470
Peterson, B. M., Ali, B., Horne, K., Bertram, R. Lame, N. J., Pogge, R. W., & Wagner, R. M. 1993, ApJ, 402, 469
Peterson, B. M., et al. 1994, ApJ, 425, 622
Peterson, B. M., Pogge, R. W., Wanders, I., Smith, S. M., & Romanishin, W. 1995, PASP, 107, 579
Reichert, G. A., et al. 1994, ApJ, 425, 582
Salamanca, I., et al. 1994, A&A, 282, 742
Schmidt, M., & Green, R. F. 1983, ApJ, 269, 352
Shields, J. C., Ferland, G. J., & Peterson, B. M. 1995, ApJ, 441, 507
Stirpe, G. M., et al. 1994, ApJ, 425, 609
Ulrich, M.-H., et al. 1991, ApJ, 382, 483
van Groningen, E., & Wanders, I. 1992, PASP, 104, 700
Wanders, I., et al. 1993, A&A, 269, 39
White, R. J., & Peterson, B. M. 1994, PASP, 106, 879
Winge, C., Peterson, B. M., Horne, K., Pogge, R. W., Pastoriza, M. G., & Storchi-Bergmann, T. 1995, ApJ, 445, 680
Winge, C., Peterson, B. M., Pastoriza, M. G., & Storchi-Bergmann, T. 1996, ApJ, 470, in press